scientific reports

Check for updates

OPEN

Ammonium capture Kinetic, Capacity, and Prospect of Rice Husk Biochar produced by different pyrolysis conditions

Yun-Gu Kang[1,4], Do-Gyun Park[1,2,4], Jun-Yeong Lee[1], Jiwon Choi[1], Jun-Ho Kim[1], Ji-Hoon Kim[1], Yeo-Uk Yun[1,3]✉ & Taek-Keun Oh[1]✉

This study explores the potential application of rice husk biochars, categorized by their pH (acidic, pH 5.98; neutral, pH 7.02; and alkali, pH 11.21) and particle sizes (micron-scale and sub-centimeter) in aquatic ecosystems for efficient removal of ammonium (NH_4^+). To assess the NH_4^+ adsorption capacity of the rice husk biochars, both NH_4^+ adsorption kinetics and isotherms were employed. Additionally, we propose future prospects for utilizing rice husk biochar as an efficient adsorbent based on a review of previous studies. Our findings suggest that the NH_4^+adsorption capacity of rice husk biochars is primarily influenced by their surface characteristics, specifically surface area of rice husk biochars and loss of acidic functional groups. In this study, the neutral rice husk biochars, which had the highest surface area at 9.86 $m^2\ g^{-1}$, exhibited the highest NH_4^+adsorption performance at 1.12 mg g^{-1} (micron-scale) and 0.94 mg g^{-1} (sub-centimeter) compared to acidic and alkali rice husk biochars. Additionally, particle size control proves to be a promising strategy for enhancing adsorption efficiency of rice husk biochars, with the micron-scale rice husk biochars being 1.19-fold higher than sub-centimeter ones. However, before implementing biochar-based pollutant removal strategies in aquatic ecosystems, several considerations (e.g., the potential harmfulness of inner components in biochar, side effects of biochar on aquatic life, and tracking the fate of biochar in aquatic ecosystems) must be addressed. By addressing these concerns, we can expect to expand the practical application of biochar for remediation in aquatic environments, contributing to the effective management of pollutants.

To address the increasing global food demand, several farmers worldwide have been urged to increase their use of chemical fertilizers (or inorganic fertilizers) to enhance crop yields[1]. During the cropping season, soil tillage, irrigation, and heavy rainfall induce the leaching of soluble nitrogen (N), resulting in increased N losses from agricultural soils as tillage, irrigation, and rainfall increase. Environmental contamination, particularly in aquatic ecosystems, resulting from N runoff, has been documented in numerous previous studies[2–4], highlighting the importance of management practices to achieve the Sustainable Development Goals (SDGs) related to clean water (Goal 6), food security (Goal 2), and environmental remediation (Goal 14 and Goal 15)[5,6]. Nitrate ions (NO_3^-) represent a soluble form of N that leaches from agricultural soils into aquatic ecosystems, including rivers, lakes, and reservoirs[4]. NO_3^- leached into aquatic ecosystem is converted to ammonium ions (NH_4^+) under acidic conditions, and as water pH becomes more alkaline, NH_4^+ volatilizes into ammonia (NH_3) gas. The above-mentioned reactions follow the Eqs. 1 and 2. These processes were activated with the alkali pH conditions (a range of pH 7.0 to pH 10.5), while they slightly decreased under the high-alkaline environment (i.e., above pH 11.0).

$$NO_3^- + 10H^+ + 8e^- \rightarrow NH_4^+ + 3H_2O \quad (1)$$

[1]Department of Bio-Environmental Chemistry, College of Agricultural and Life Science, Chungnam National University, Daejeon 34134, South Korea. [2]Rural Development Administration, National Institute of Agricultural Sciences, Wanju 55365, South Korea. [3]Division of Environmentally Friendly Agriculture, Chungcheongnam-do Agricultural Research and Extension Services, Yesan 32418, South Korea. [4]Yun-Gu Kang and Do-Gyun Park contributed equally to this work. ✉email: aoggi61@korea.kr; ok5382@cnu.ac.kr

$$NH_4^+ + OH^- \rightarrow NH_3 + H_2O \quad (2)$$

In uncontaminated aquatic ecosystems, NH_4^+typically exists in small quantities. However, its concentration can increase when supplied from various sources of contamination (e.g., agricultural soils, industry, household, and etc.) or due to acidification of aquatic ecosystems, leading to adverse effects such as fish kills, eutrophication, toxic algal blooms, and blue-baby syndrome[7–9]. Additionally, NH_4^+ can be released into atmospheric ecosystems as NH_3 gas, contributing to the formation of secondary particulate matter, commonly abbreviated to $PM_{2.5}$[6]. Apart from converting NH_4^+ into NH_3 gas, the agricultural residues, organic fertilizers, and animal-based compost also caused NH_3 volatilization in agricultural soils. Given these concerns, there is an urgent need to develop more efficient strategies for NH_4^+ removal in polluted or acidic aquatic ecosystems.

In recent years, there has been a rapid increase in research related to biochar in agricultural and environmental fields. Numerous studies have investigated the use of biochar as an adsorbent for removing $NH_4^+$from aquatic environments[9–12].

For instance, a previous study evaluated the removal efficiency of orange peel biochar for bismuth (Bi) in a Bi-containing solution (Table 1). It documented that Bi adsorption was influenced by electrostatic attraction, ion exchange, and the complexation of -OH and -COOH groups on orange peel biochar[13].

Another previous study evaluated the NH_4^+adsorption characteristics of pine sawdust and wheat straw biochars under different pyrolysis conditions[14]. They reported that the optimal pyrolysis conditions for NH_4^+adsorption efficiency varied depending on the biochar feedstock. The aforementioned previous studies also reported that the adsorption capacity of biochar varies with the feedstock, pyrolysis conditions, and physicochemical properties of biochar[13–24]. Therefore, it is necessary to evaluate the adsorption characteristics by altering the properties of biochar.

Biochar was produced using rice husk, a widely used material in previous studies, and its adsorption characteristics (i.e., kinetic and capacity) for NH_4^+ were evaluated. The rice husk biochar was ground to distinguish its physical properties at the micron-scale (< 0.53 μm) and sub-centimeter levels (< 1.0 cm), while variations in pyrolysis temperature and duration were employed to differentiate its chemical properties (e.g., pH, surface area, and carbon content). This study hypothesized that the pyrolysis conditions of rice husk biochar would alter its physicochemical properties, thereby affecting its NH_4^+ adsorption capacity in aqueous state. Based on this assumption, the changes in adsorption kinetic and capacity resulting from these altered properties were evaluated. Therefore, the ultimate goal is to provide insights into potential application strategies of rice husk biochar as an efficient adsorbent for removing NH_4^+ from polluted or acidic aquatic ecosystems.

Results

Chemical characteristics of rice husk biochars varied by the pyrolysis conditions

Table 2. exhibits the chemical properties, such as pH, electrical conductivity (EC), BET surface area, and elemental compositions (i.e., carbon, hydrogen, nitrogen, oxygen, and phosphorus), of the rice husk biochars and their corresponding pyrolysis temperature and time (hour, h). This study aims to classify the rice husk biochars by their pH values, and various pyrolysis conditions were assessed before conducting the NH_4^+ adsorption experiment (as shown in Table S1 of the Supplementary materials). The pH of the rice husk biochars was gradually increased with higher pyrolysis temperatures (from 350 to 600 °C) and extended durations (from 0.25 h to 0.50 h). The acidic rice husk biochar (pH 5.98) was not observed the significant difference with the pH of rice husk (pH 6.04), while the neutral (pH 7.02) and alkali (pH 11.21) rice husk biochars had the higher pH values compared to the rice husk. Although the pH variations in the acidic and neutral rice husk biochar were relatively small, at pH 6.04 and pH 7.02, respectively, they serve as a representative example of how the chemical characteristics of biochar can change depending on the pyrolysis conditions. hese change also affected in the adsorption characteristics of the rice husk biochars. In contrast, the EC values of the rice husk biochars were decreased as their corresponding pyrolysis conditions were declined. The alkali rice husk biochar exhibited the lowest EC values at 5.69 dS m^{-1}, while the acidic and neutral rice husk biochars were quantified at 10.51 dS m^{-1} and 9.35 dS m^{-1}, respectively. The BET surface area of acidic, neutral, and alkali rice husk biochars was 2.85 m^2 g^{-1}, 9.86 m^2 g^{-1}, and 8.30 m^2 g^{-1}, respectively, with the neutral rice husk biochar having the highest value compared to the acidic and alkali rice husk biochars. The total carbon (TC), total nitrogen (TN), and total phosphorus (TP) contents of the alkali rice husk biochar increased with reinforced pyrolysis conditions (i.e., 600 °C and 0.5 h), while the TN and TP contents did not exhibit the statistically significant differences among the acidic, neutral, and alkali rice husk biochars. The alkali rice husk biochar consisted of TC 59.45%, TN 0.56%, and TP 0.25%, while the acidic and neutral rice husk biochars composed of TC 42.13%, TN 0.32%, and TP 0.15% and TC 45.14%, TN 0.45%, and TP 0.21%, respectively. On the other hand, the total hydrogen (TH) and total oxygen (TO) contents decreased with the increase in the pyrolysis temperature and time of the rice husk biochars, with the highest values observed in the acidic rice husk biochar at 5.35% and 35.17%, respectively. The alkali rice husk biochar, which had the lowest values of TH and TO contents, was analyzed at 1.99% and 4.89%, respectively. The H: C ratio and O: C ratio, which indicated the aromaticity and polarity of the rice husk biochars, decreased with reinforced pyrolysis temperature and duration. The H: C ratio and O: C ratio of the alkali rice husk biochar were observed at 0.40 and 0.06, respectively, while the acidic and neutral rice husk biochars had values three and five times higher, respectively.

The FT-IR results, containing the functional groups on the rice husk biochar surface, are shown in Fig. 1. The -NH and $-NH_2$ bonds (3325 cm^{-1}), representing secondary amide groups, were recorded in the acidic rice husk biochar, while the neutral and alkali rice husk biochars did not show the above-mentioned peak. Similarly, $-CH_3$ and -CH bonds were rapidly disappeared with the higher temperature and longer duration of pyrolysis process. Reinforced pyrolysis conditions induced to formation of the C-based specific bonds, including C-C, C=C,

Feedstocks	Pyrolysis conditions		Maximum capacity (mg g− 1)	Factors affecting target adsorption	Adsorption mechanism	References
	Temperature (°C)	Time (h)				
Oak tree	500	3.0	1.94	Surface characteristics, initial solution concentration,	Surface sorption and multiple adsorption	[13]
Pine sawdust	300	2.0	5.38	Feedstock, application rate, biochar pH, initial solution concentration, and competing ions in NH_4^+-solution	Chemical bonding, electrostatic attraction, and surface sorption	[14]
	550	2.0	3.37			
Wheat straw	550	2.0	2.08			
Rice husk	330,	0.3	7.26	Pyrolysis temperature and duration, biochar pH, surface area of biochar, and solution concentration	Electrostatic attraction and surface sorption	[15]
	400	0.3	10.46			
	600	0.5	31.55			
	600	10.0	133.33	Biochar dosage and pH, initial effluent concentration, biochar particle size, and contact time	ionic bond formation with surface functional groups and surface area dependent physical diffusion	[16]
Mixed wood cuttings	600	10.0	71.94			
Giant reed straw	500	2.0	1.40	Initial solution concentration, solution temperature, biochar pH, ionic strength, and contact time	ion exchange and surface area	[17]
Maize stalk	300	1.0	2.72	Feedstock, pyrolysis temperature, surface functional groups, biochar pH, and H: C ratio	Electrostatic attraction, cation exchange, functional groups, and surface sorption	[18]
	400		1.15			
	500		1.09			
	600		0.04			
	700		0.01			
Maize cob	300	1.0	1.29			
	400		0.78			
	500		0.28			
	600		0.10			
	700		0.02			
Rice straw	300	1.0	1.69			
	400		0.53			
	500		0.25			
	600		0.13			
	700		0.13			
Rice husk	300	1.0	0.32			
	400		0.32			
	500		0.08			
	600		0.05			
	700		0.05			
Pine needles	300	0.5	0.07	Pyrolysis temperature, surface characteristics, and Mesopore formation	Electrostatic attraction and surface sorption	[19]
		2.0	0.02			
	400	0.5	0.03			
		2.0	0.01			
	500	0.5	0.01			
		2.0	0.01			
Oak sawdust	300	0.5	5.31	Acidic functional groups, O/C and (O + N)/C ratios	Electrostatic attraction and surface sorption	[20]
Peanut shell	500	2.0	24.58	Acidic functional groups and surface characteristics	Electrostatic attraction, hydrogen-bond interaction, and surface sorption	[21]
Wheat straw	500	1.5	0.63	Feedstock and pyrolysis temperature	Electrostatic interaction and cation exchange	[22]
Corn straw			2.12			
Peanut shell			0.73			
Wheat straw	600	1.0	0.95	Initial solution concentration	Van der Waals' force, hydrogen-bond interaction, ion-dipole interaction, and hydrophobic interaction	[4]
Sesame straw	300	2.0	3.45	Surface functional groups and pyrolysis temperature	Electrostatic interaction and functional groups (-OH and -COOH)	[23]
	500		0.91			
	700		1.62			
Corn cob	400	2.0	15.3	Surface area of biochar, pyrolysis temperature, and surface polar functional groups,	Hydrogen-bond interaction	[24]
	600		12.8			

Table 1. Pyrolysis conditions, adsorption characteristics and mechanism of several ions on different biochars.

Rice husk biochars	Pyrolysis conditions		pH	EC	BET surface area	Elemental components					H: C ratio	O: C ratio
	Temp.	Duration				TC	TN	TH	TO	TP		
	(°C)	(h)	(1:10, H_2O)	(dS m^{-1})	(m^2 g^{-1})	(%)						
Acidic	350	0.25	5.98 ± 0.03c	5.69 ± 0.13c	2.85 ± 0.12c	42.13 ± 0.22b	0.32 ± 0.02c	5.35 ± 0.07a	35.17 ± 0.16[a]	0.15 ± 0.01[a]	1.51	0.63
Neutral	450	0.25	7.02 ± 0.05b	9.35 ± 0.25b	9.86 ± 0.20a	45.14 ± 0.15b	0.45 ± 0.01b	5.29 ± 0.13a	33.21 ± 0.33[a]	0.21 ± 0.02[a]	1.40	0.55
Alkali	600	0.50	11.21 ± 0.06a	10.51 ± 0.17a	8.30 ± 0.31b	59.45 ± 0.19a	0.56 ± 0.03a	1.99 ± 0.09b	4.89 ± 0.29[b]	0.25 ± 0.01[a]	0.40	0.06
p-value			**	**	**	**	*	***	***	**	-	-

Table 2.. Pyrolysis conditions and chemical properties of rice husk biochars. Temp., temperature; EC, electrical conductivity; TC, total carbon; TN, total nitrogen; TH, total hydrogen; TO, total oxygen; TP, total phosphorus. a-c: Each value with different letters within a column are significantly different from each other as determined by Duncan's multiple range test. *, **, and *** denote the statistically significant differences (p) at $p < 0.05$, $p < 0.01$, and $p < 0.001$, respectively, based on the Duncan's multiple range test.

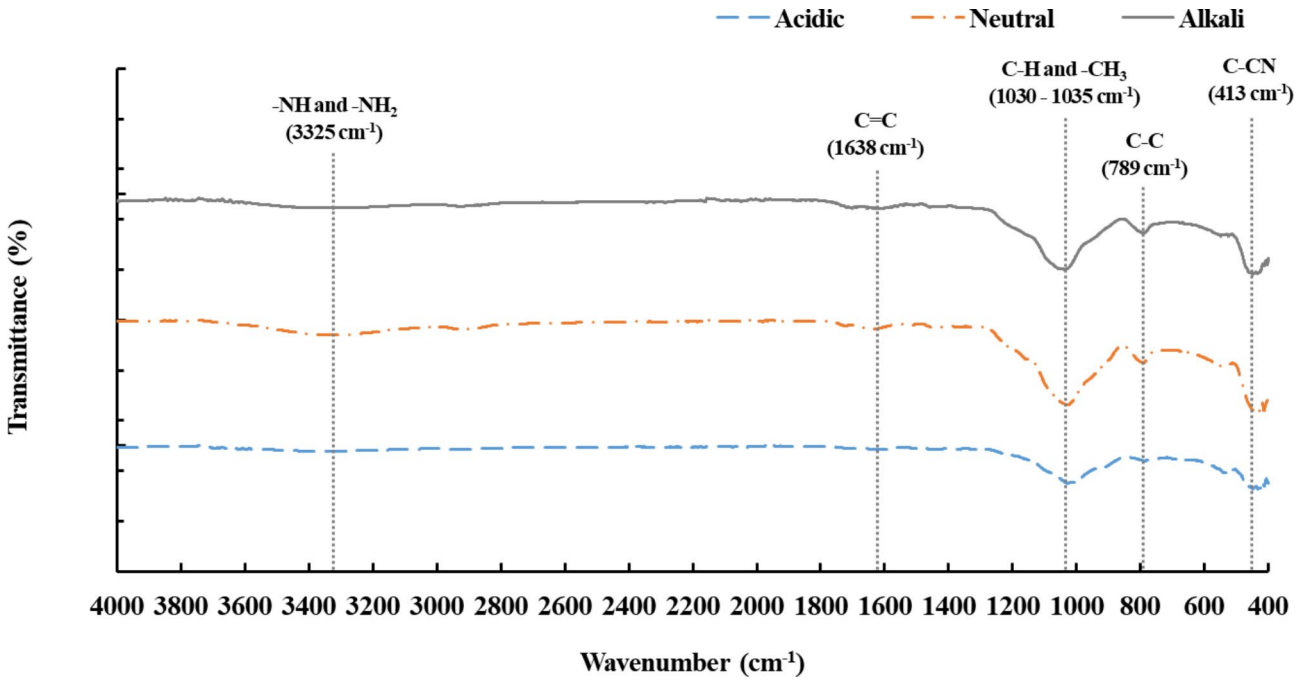

Fig. 1. FT-IR spectrum of the rice husk biochars sorted by their pH values.

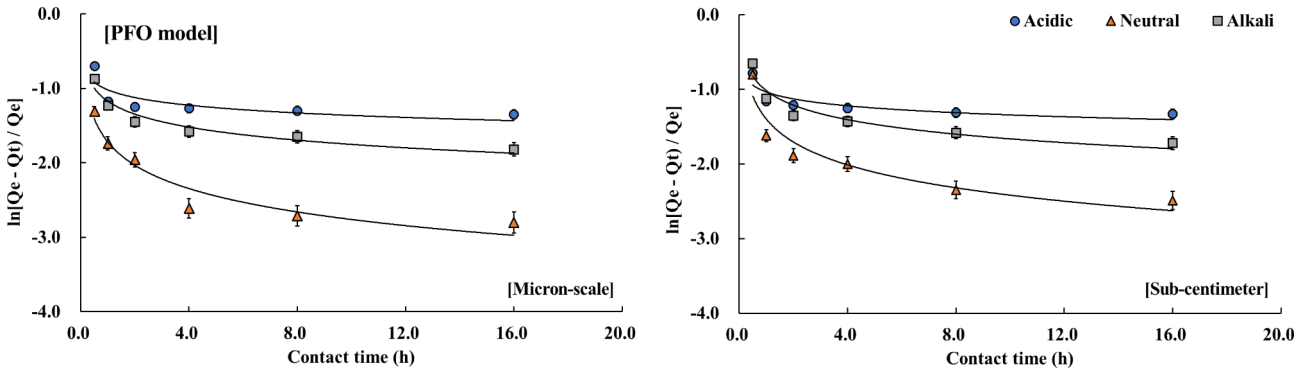

Fig. 2. Kinetic curves of the rice husk biochars categorized as their particle size and pH values based on Pseudo-first-order model.

and -C-CN bonds, and C accumulation in the form of multiple connections. This mean that the abundance of the functional groups on rice husk biochar's surface increased with higher pyrolysis temperature and longer pyrolysis time.

The NH_4^+ adsorption kinetic of the rice husk biochars

The NH_4^+adsorption rates by the different rice husk biochars were assessed using the varying forms of the pseudo-first-order (PFO) and pseudo-second-order (PSO) models proposed in previous study[14]. These results were evaluated using the coefficient of determination (R^2), which indicates the explanatory ability of kinetic performance. Figure 2 illustrates the kinetic characteristics of the micron-scale and sub-centimeter rice husk biochars classified by their pH values based on the PFO model, while Fig. 3 shows the results subjecting the PSO model.

In the PFO model, the kinetic curves of the micron-scale and sub-centimeter rice husk biochars exhibited duality, with the micron-scale rice husk biochar reaching equilibrium at 2 h after the reaction, while the sub-centimeter rice husk biochar attained at 1 h after the reaction (Fig. 2). It indicates that the NH_4^+adsorption rates were affected by the particle size of the rice husk biochars, with smaller particle size leading to longer adsorption durations and higher adsorption amount (Table S2 in the Supplementary materials). However, in this study, the PFO model had the lower R^2 value for all kinetic data compared to the PSO model, indicating the PSO model was more suitable for interpreting the kinetic data of this study (Fig. 3).

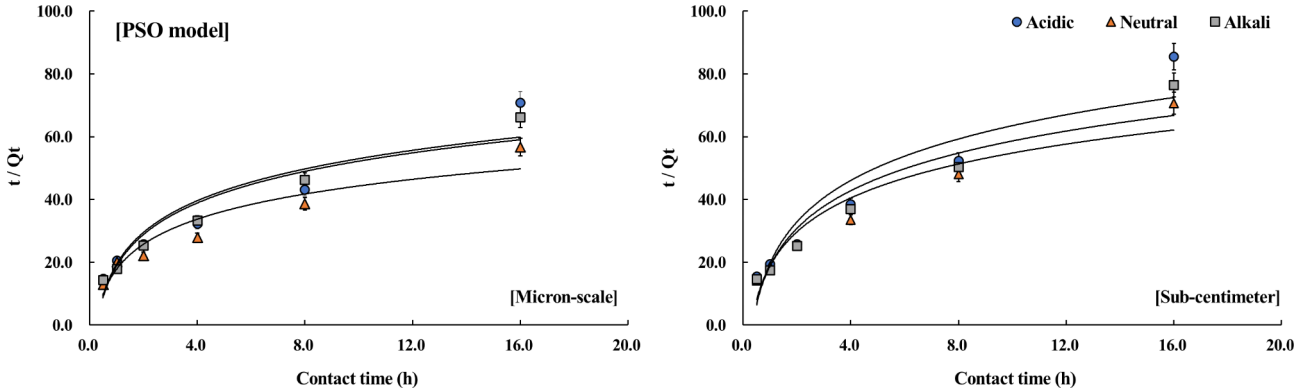

Fig. 3. Kinetic curves of the rice husk biochars categorized as their particle size and pH values based on Pseudo-second-order model.

Rice husk biochars		K2	Qe	h	R2
Particle size	pH	(g mg− 1 h− 1)	(mg g− 1)		
Micron-scale	Acidic	0.31	0.29	0.06	0.99
	Neutral	0.54	0.38	0.06	0.98
	Alkali	0.36	0.31	0.06	0.99
Sub-centimeter	Acidic	0.19	0.23	0.06	0.99
	Neutral	0.29	0.28	0.06	0.98
	Alkali	0.24	0.26	0.06	0.98

Table 3. Kinetic parameters of NH_4^+ adsorption process on the rice husk biochars for pseudo-second-order model. K_2, kinetic constant of Pseudo-second-order model; Q_e, total amount of NH_4^+adsorbed by the rice husk biochars; h, initial adsorption rate; R^2, coefficient of determination.

The kinetic parameters, including the K_2, h, and Q_e values, of the PSO model over the entire adsorption duration are listed in Table 3. The estimated K_2 values were 0.31 g mg^{-1} h^{-1}, 0.54 g mg^{-1} h^{-1}, and 0.36 g mg^{-1} h^{-1} for the micron-scale rice husk biochar with acidic, neutral, and alkali pH, respectively, while the K_2 values of the sub-centimeter rice husk biochars were calculated as 0.19 g mg^{-1} h^{-1} (acidic), 0.29 g mg^{-1} h^{-1} (neutral), and 0.24 g mg^{-1} h^{-1} (alkali). Similarly, the NH_4^+ adsorption rate, defined as K_2 values, was higher in the micron-scale rice husk biochar than the sub-centimeter rice husk biochar, and it was superior in the neutral rice husk biochar compared to the acidic and alkali rice husk biochars. However, the h parameter and R^2 value of each rice husk biochar did not exhibit significant differences. The amount of NH_4^+ adsorbed by the rice husk biochars at equilibrium (Q_e) was the highest in the micron-scale neutral rice husk biochar at 0.38 mg g^{-1}, and the Q_e values decreased with an increase in the particle size of the rice husk biochars. Additionally, the alkali rice husk biochar was higher than the acidic rice husk biochar in both micron-scale and sub-centimeter. Unlike K_2 and Q_e values, the constant h, which indicates the initial NH_4^+ adsorption rate and is calculated by K_2 and Q_e values, did not show significant differences in all treatments.

The NH_4^+ adsorption capacity of the rice husk biochars

The adsorption capacity of NH_4^+ varied depending on the physicochemical properties of the rice husk biochars, such as particle size, pH, and BET surface area. The above-mentioned findings are illustrated in Figs. 4 and 5, with Fig. 4 representing the linear form of the Freundlich isotherm and Fig. 5 obtained from the Langmuir isotherm. Additionally, Tables 4 and 5present the experimental parameters of both Freundlich and Langmuir isotherms, derived from the corresponding isotherm curves. The findings of this study, which revealed similarly high R^2 values between the Freundlich and Langmuir isotherms, indicated that the NH_4^+adsorption by chemical interactions (e.g., van der Waals interactions and hydrogen bonding) and monolayer adsorption of the rice husk biochars occurred simultaneously[3].

In the Freundlich isotherm, the NH_4^+ adsorption capacity (K_F) of the rice husk biochars was higher in the micron-scale rice husk biochars than in the sub-centimeter ones. The neutral pH of the rice husk biochar led to the highest K_F values at 3.39 (micron-scale) and 3.00 (sub-centimeter) within the same particle size categories. The acidic and alkali rice husk biochars were observed at 2.89 and 3.29 with the micron-scale, while the sub-centimeter acidic and alkali rice husk biochars were calculated at 1.39 and 2.92, respectively (Table 4). However, the parameter n, which denotes the NH_4^+ adsorption strength of rice husk biochar, did not showed differences in the same pH levels of the rice husk biochar between micron-scale and sub-centimeter ones. The neutral rice husk biochar was represented the highest n values at 0.12, while the acidic and alkali rice husk biochars represented values of 0.10 and 0.11, respectively.

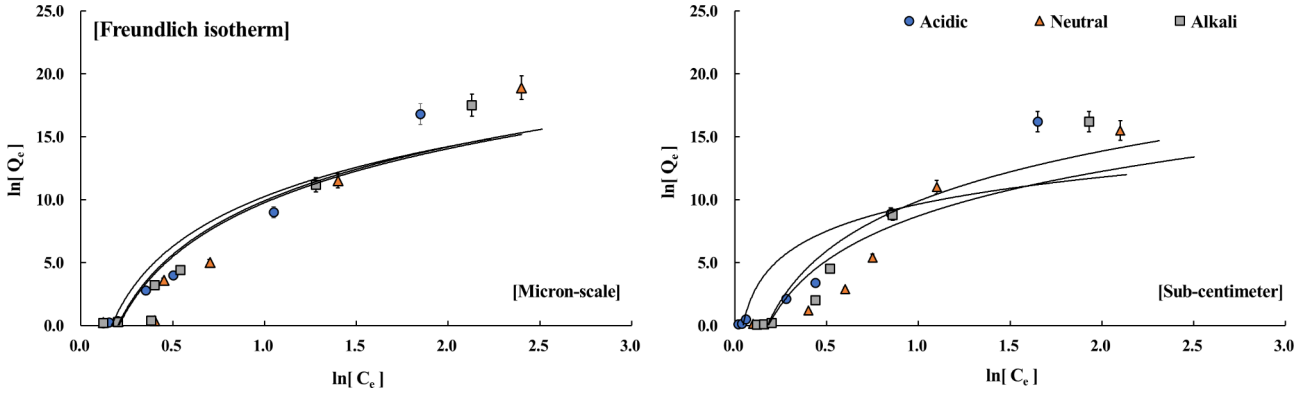

Fig. 4. Effects of particle size and pH of the rice husk biochars based on the Freundlich isotherm.

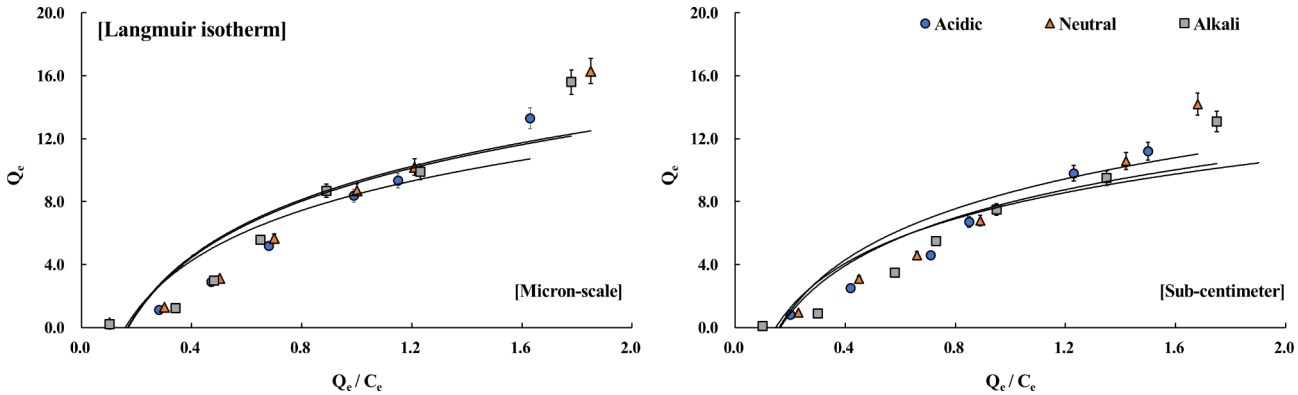

Fig. 5. Effects of particle size and pH of the rice husk biochars based on the Langmuir isotherm.

Micron-scale	Acidic	2.89	0.10	0.99
	Neutral	3.39	0.12	0.98
	Alkali	3.29	0.11	0.98
Sub-centimeter	Acidic	1.39	0.10	0.99
	Neutral	3.00	0.12	0.94
	Alkali	2.92	0.11	0.97

Table 4. Parameters of Freundlich isotherm for the NH_4^+ adsorption onto the rice husk biochars. KF, adsorption capacity constant in Freundlich isotherm; n, adsorption intensity constant in Freundlich isotherm; R^2, coefficient of determination.

The NH_4^+ adsorption rates (Q_m) were higher in the micron-scale rice husk biochars, with the values of 0.98 mg g^{-1}, 1.12 mg g^{-1}, and 1.05 mg g^{-1} according to the pH of the rice husk biochars (Table 5). In the sub-centimeter rice husk biochars, the Q_m values were 0.82 mg g^{-1} (acidic), 0.94 mg g^{-1} (neutral), and 0.88 mg g^{-1} (alkali). The parameter b, which represents the binding capacity of the rice husk biochars, did not show significant differences among the acidic, neutral, and alkali rice husk biochars, while the micron-scale rice husk biochar was higher than the sub-centimeter ones.

The dimensionless constant (R_L), which represents that the favorability of the Langmuir isotherm, was estimated to be 0.09 and 0.08 (especially, the suitable range is $0 < R_L < 1$) for the micro-scale and sub-centimeter rice husk biochars, respectively (Table S3 in the Supplementary materials). Nevertheless, the R^2 value did not exhibit significant differences across the physicochemical properties of the rice husk biochar, remaining consistently high at 0.99.

Rice husk biochars		Q_m	b	R^2
Particle size	pH	(mg g^{-1})	(L mg^{-1})	
Micron-scale	Acidic	0.98	0.11	0.99
	Neutral	1.12	0.11	0.99
	Alkali	1.05	0.11	0.99
Sub-centimeter	Acidic	0.82	0.12	0.99
	Neutral	0.94	0.12	0.99
	Alkali	0.88	0.12	0.99

Table 5. Parameters of Langmuir isotherm for the NH_4^+ adsorption onto the rice husk biochars. Q_m, monolayer adsorption capacity of NH_4^+ by rice husk biochars; b, binding capacity of rice husk biochar; R^2, coefficient of determination.

Discussion

Pyrolysis temperature and time regulated the chemical properties of the rice husk biochars

The rice husk biochars utilized in this study were categorized according to their pH values, namely acidic (pH 5.98), neutral (pH 7.02), and alkali (pH 11.21), which primarily represented the different pyrolysis conditions. In this study, the acidic rice husk biochar exhibited a lower pH value than the feedstock, which had a slightly acid pH of 6.27 (Table S1). This was because acidic volatile substances (e.g., acetic acid and phenolic compounds) did not evaporate at the relatively low temperature (especially below 470℃) and short duration[25]. However, as the pyrolysis temperature and duration increased, the rise in the pH of the rice husk biochars from acidic to alkali associated with the loss of the TH content and the formation of aromatic carbon as shown by Table 2.; Fig. 1, respectively. The previous studies have reported that the H and O content in biochar volatilizes during the pyrolysis process in the form of steam (i.e., H_2O), carbon dioxide, and hydrocarbons, leading to the loss of acidic O-containing functional groups (e.g., carboxyl group)[26,27]. Additionally, it is known that these reactions primarily occur at temperatures above 500 °C, where lignin is decomposed[26]. In this study, the TH content in the rice husk biochar decreased as the pyrolysis conditions intensified, which led to the disappearance of $-CH_3$ and -CH peaks in the FT-IR results (Fig. 1). This loss of alkyl groups (e.g., $-CH_3$and -CH) indicates the conversion long-chain C bonds to relatively short-chain C bonds or aromatic structure on the biochar surface. These findings are supported by several previous studies that have recorded the alkali effects of biochar[15,27]. Furthermore, the alkali effects of biochar were evident in the changes in the TP content, which is a representative alkaline element, of the rice husk biochars. The EC values utilize to indicate the concentration of total dissolved salt and soluble alkaline cations in biochar, and it was generally known as having positive (+) correlation with pyrolysis conditions[18,22]. Specifically, these increases were attributed to the highly available salt content and loss of the acidic functional groups of biochar[22]. The findings of this study agreed to the previous studies, where was that the EC values of the rice husk biochar increased by the reinforced pyrolysis conditions.

Previous studies have noted that the BET surface area of biochar, a major factor influencing adsorption characteristics, increases with rising pyrolysis temperature and time, within a range of 300 °C to 600 °C[28–30]. Additionally, the pyrolysis process based on plant residues resulted in higher residual substances (e.g., ash, tar, and vinegar), which can interfere with the development of micropores on the biochar surface[29]. The formation of relatively thin pore walls and the impairment of the porous structure, leading to reduced adsorption capacity of biochar, also result from high pyrolysis conditions (especially above 600 °C)[28]. In this study, the BET surface area of the rice husk biochar decreased with the increase in the pyrolysis temperature from 450 °C (neutral) to 600 °C (alkali), consistent with findings from previous studies[6,15,28–30]. This decrease was attributed to the competing-relationship between the porous structure formation and pores loss on the surface of the rice husk biochars under the high pyrolysis conditions[30]. Additionally, the declined removal rate of volatile substances under these conditions contributed to the above-mentioned findings with the increase in the pyrolysis conditions[30].

The TN content of the rice husk biochars showed a positive (+) correlation with the pyrolysis conditions, with the alkali rice husk biochar having a higher TN content than the acidic and neutral rice husk biochars. Findings by Jassal et al. (2015) and Kang et al. (2024) highlighted that N-containing groups condensed into C-based bonds (e.g., aromatic and hetero-ring structures), while the H and O contents were rapid decreased under the high pyrolysis temperatures[15,31]. These findings were connected the changes in the H: C and O: C ratios in the rice husk biochar, where the H: C ratio and O: C ratio were decreased from 1.55 to 0.46 and from 0.63 to 0.08, respectively, with the reinforced pyrolysis conditions (Table 2.). The above-mentioned findings indicate that high temperatures and prolonged durations during the pyrolysis process significantly affected the aromaticity and polarity of biochar, resulting in the strong formation of hydrophobic characteristics and aromatic structure[32]. Actually, a low O: C ratio in the rice husk biochars indicates high aromatic characteristics, leading to strong NH_4^+adsorption capacity rather than a high adsorption rate, where its aromatic structure could explain the C accumulation under relatively high pyrolysis conditions[15,33]. These results are consistent with those obtained by several previous studies[15,18,34,35]. For example, Ippolito et al. (2020) reported that H: C and O: C ratios were key factors in describing the environmental longevity of biochar, and they increased under reinforced pyrolysis conditions (especially temperature) with the loss of H and O in the form of gas (e.g., H_2O, CO_2, and hydrocarbon)[35].

The NH_4^+adsorption rate and capacity affected by the particle size and pH of rice husk biochar

In this study, the NH_4^+ adsorption rates varied with the pH values of the rice husk biochars under the neutral solution conditions. However, the NH_4^+ adsorption capacity was closely aligned with the BET surface area of the rice husk biochars, suggesting that their surface characteristics primarily influenced the NH_4^+ adsorption capacity. The NH_4^+adsorption capacity of the acidic (BET surface area, 2.85 $m^2\ g^{-1}$), neutral (9.86 $m^2\ g^{-1}$), and alkali (8.30 $m^2 g^{-1}$) rice husk biochars was 0.98 mg g^{-1}, 1.12 mg g^{-1}, and 1.05 mg g^{-1} in the micron-scale, respectively, while those of the sub-centimeter were quantified as 0.82 mg g^{-1}, 0.94 mg g^{-1}, and 0.88 mg g^{-1}, respectively (Table 5). These findings are supported by previous study[29], who included scanning electron microscope (SEM) image results of rice husk biochars at three pyrolysis temperature conditions. The aforementioned study noted that the pore structure of rice husk biochar pyrolyzed at 350 °C was not fully developed, while it was destroyed at pyrolysis temperatures above 600 °C[29,34]. Generally, the pore structure of rice husk biochar forms a honeycomb-like structure up to a pyrolysis temperature of 500 °C[36]. Additionally, previous research reported on the mechanisms for NH_4^+ adsorption by surface characteristics of rice husk biochar and illustrated that its NH_4^+ adsorption occurs mainly through cation H^+on O-containing function groups on the biochar surface, depending on the pyrolysis conditions[33]. These findings indicate that the neutral rice husk biochar, with the highest BET surface area and well-built pore structure (i.e., honeycomb-like structure), exhibit the superior NH_4^+ adsorption performance in aquatic ecosystems compared to acidic and alkali rice husk biochar.

Regarding NH_4^+ adsorption by biochar, various previous studies have noted that the NH_4^+adsorption capacity of biochar varies depending on the factors, including feedstocks, pyrolysis conditions (i.e., temperature)[14,15], physicochemical properties (e.g., pH, BET surface area, and functional groups)[15,23,37,38], and interaction characteristics (e.g., ionic strength, van der Waals interaction, and hydrogen bonding)[18,21–24], and ranged widely from 0.01 mg g^{-1} to 518.90 mg g^{-1}. Additionally, other studies have shown that the adsorption capacity of biochar is affected not only by the above-mentioned factors but also by particle size, ion competition, aromaticity, polarity, and pore size[14,16]. In this study, the particle size (i.e., micron-scale and sub-centimeter) of the rice husk biochars significantly affected the NH_4^+ adsorption performance, with higher NH_4^+adsorption performance observed in the micron-scale rice husk biochars. Regulating the particle size of biochar is recognized as an effective physical method to enhance its adsorption capacity[38]. Specifically, for a unit mass of biochar, the micron-scale rice husk biochar has a larger surface area and contains more microspores compared to the sub-centimeter-sized rice husk biochar, which leads to better adsorption performance[39,40]. These findings are supported by previous study[41], who noted that smaller biochar sizes result in more collisions with the adsorbate (NH_4^+), resulting from the increase in their adsorption capacity than larger sizes. Actually, in this study, the NH_4^+ adsorption capacity of the acidic and alkali rice husk biochars in the sub-centimeter was higher than the micron-scale neutral rice husk biochar (Table 5). Therefore, reducing the particle size of the rice husk biochar from sub-centimeter to micron-scale appears to be a highly feasible strategy for enhancing its NH_4^+ adsorption capacity and NH_4^+removal efficiency in aquatic ecosystems. However, these practices need to consider the exposure risk of relatively small particles to various organisms (e.g., fish, plankton, and aquatic plants) in aquatic ecosystems[42]. Although a few studies reported on the influence of micron-scale biochar on organisms[43,44], the possibility of ecological toxicity was remains.

Future prospective and utilization of the rice husk biochars as an efficient adsorbent

Initial studies on biochar application focused on its utilization as a soil amendment to enhance crop yield, mitigate greenhouse gases (e.g., nitrous oxide), regulate soil pH, and sequester C content[6,18,26,27]. These findings led to the potential utilization of biochar for removing several pollutants as an adsorbent in aquatic ecosystems, owing to its unique characteristics of biochar, including various surface functional groups, specific pollutants (e.g., NH_4^+, NO_3^-, and heavy metals) adsorption, and properties optimization[15,45]. However, there are significant constraints and safety standards to consider before implementing biochar-based pollutant removal strategies in aquatic ecosystems.

Firstly, the effects of potentially harmful components in biochar on various organisms and the environments must be taken into account. Previous study has noted that biochar contains the polycyclic aromatic hydrocarbons (PAHs), dioxin, environmentally persistent free radicals (EPFRs), and perfluorocarbons (PFCs), and volatile organic compounds (VOCs), which can cause various environmental issues during the pyrolysis process[45]. These pollutants can accumulate in aquatic organisms and environments, potentially leading to harmful effects on higher organisms (e.g., human) through the aquatic food chain. Several laboratory-scale studies have not fully explored the correlation or resolved the effects of these pollutants from long-term biochar application in aquatic ecosystems[46,47]. Therefore, further studies are needed to reduce the effects of specific pollutants contained in biochar.

Secondly, the potential risks by direct exposure of biochar, such as feeding, on aquatic organisms must be fully considered. Most previous studies, conducted in controlled environments, have not adequately addressed the negative biotic/abiotic effects of biochar on aquatic organisms, including plankton, protozoa, and fishes. A previous study reported that substances introduced from the external environments, including biochar, negatively affected algae growth, but the specific mechanisms of the above-mentioned effects have not been elucidated[44]. Furthermore, another study noted that algae were negatively affected by biochar attachment to cell surfaces, inducing the oxidant injury, with the degree of acute toxicity determined by pyrolysis conditions and particle size[48]. Additionally, biochar consumed by fish can accumulate through the aquatic food chain, potentially posing undisclosed health risks to humans. Therefore, further studies are needed to mitigate environmental and health risks associated with biochar through control of pyrolysis conditions, modification, and particle size in larger-scale experiments.

Lastly, tracking and understanding biochar transport along water flow is important. Biochar can be transported to other locations through water flow, potentially causing further environmental pollution. Previous studies have suggested the big sensor-based tracking systems to evaluate biochar transport in aquatic ecosystems[49]. This strategy can confirm the dynamics and movement of pollutants, including biochar[49]. Recently, the techniques based on the information and communication technology (ICT) and artificial intelligence (AI) were rapidly developed across industries, offering various advantages for environmental management. Therefore, further studies are needed to combine ICT- or AI-based utilization strategies with existing environmental management practice for effective biochar tracking in aquatic ecosystems.

The following 3 points summarize the major prospects and utilization of biochar as an efficient adsorbent in aquatic ecosystems. In addition to this, the appropriate pre-treatment of biochar (e.g., washing, acid-activation, and formulation) is necessary to address the above-mentioned issues depending on the situation. For example, proper washing can remove the pollutants from the biochar surface, and biochar formulation, such as beads and pellets, can reduce the potential risks associated with direct exposure to biochar.

(1) The potential harmfulness of biochar needs to be confirmed based on the physicochemical characteristics of biochar.

(2) The field-based long-term studies needs to identify the relationship between pyrolysis conditions of biochar and aquatic organisms.

(3) The ICT- or AI-based strategies utilize effective methods for biochar tracking in aquatic ecosystems.

Conclusion

Nitrogen (N) management, particularly ammonium ion (NH_4^+), in aquatic ecosystems is important for addressing the food crisis and environmental remediation outlined in the Sustainable Development Goals (SDGs). This study explores the potential applications of the rice husk biochars, categorized by their pH values (acidic, pH 5.98; neutral, pH 7.02; and alkali, pH 11.21) and particle sizes (micron-scale and sub-centimeter), in aquatic ecosystems by evaluating their adsorption kinetics and isotherms. In addition, various previous studies were reviewed to provide the insights into both the past and future perspectives of biochar applications to the N management for sustainable agricultural environments.

In conclusion, the chemical characteristics of the rice husk biochars were affected by the varying pyrolysis temperature and duration, generally increasing with more intense pyrolysis conditions. Especially, the pH, electrical conductivity, and elemental compositions (i.e., carbon, nitrogen, and phosphorus) of the rice husk biochars were increased with higher pyrolysis temperature and longer duration, while the surface area was slightly decreased. These variations influenced the adsorption characteristics of the rice husk biochars. The NH_4^+ adsorption performance of the rice husk biochars was enhanced by a higher surface area and smaller particle size. Specifically, the NH_4^+ adsorption rate of the rice husk biochars for reaching equilibrium state was longer in the micron-scale (2.0 h) than sub-centimeter (1.0 h), leading to a higher NH_4^+adsorption capacity. When categorized by their pH values, the neutral rice husk biochar, with the highest surface area at 9.86 $m^2\ g^{-1}$, exhibited the greatest NH_4^+ adsorption performance (micron-scale: 1.12 mg g^{-1} and sub-centimeter: 0.94 mg g^{-1}) compared to the acidic and alkali rice husk biochars. Furthermore, the decrease in the particle size of the rice husk biochars from sub-centimeter to micron-scale resulted in a 1.19-fold higher adsorption capacity for NH_4^+ removal.

Therefore, rice husk biochar, having micron-scale particle size and neutral pH, appears to be the most suitable option for NH_4^+ removal in aquatic ecosystems due to its high adsorption performance. However, this study primarily focused on evaluating the NH_4^+ adsorption capacity of the rice husk biochars under controlled conditions (e.g., neutral pH of NH_4^+ solution, room temperature, and exception of any interfering substances), which differ from actual aquatic environments. This highlights the need for future studies to investigate the potential side effects on aquatic organisms and the environmental fate of rice husk biochars. These findings will contribute to the expanded practical application of rice husk biochar for remediating aquatic environments.

Materials and methods

Preparation of experimental materials

Two forms of rice husk biochar (i.e., micron-scale and sub-centimeter) for removing NH_4^+in aquatic environments were manufactured under different pyrolysis temperature (350°C, 450°C, and 600°C) and duration (0.25 h and 0.5 h). The rice husks were obtained from the experimental paddy field at Chungnam National University (36°22' 04.5" N 127°21' 15.1" E) in Daejeon, South Korea. To produce the rice husk biochars, the rice husks were washed with secondary deionized water to eliminate various impurities, including rice husk ash and vinegar, and dried at 85 °C for 48 h in a reinforced convection oven (Jeio-tech, Seoul, South Korea). The dried samples underwent pyrolysis processes under varying pyrolysis conditions using an electrical furnace (1100 °C Box Furnace, Thermo Scientific Inc., Waltham, Massachusetts, USA). The rice husk biochars were categorized based on their pH values, which were representative characteristics of biochar, indicating the varying pyrolysis conditions. The acidic rice husk biochar (pH 5.98) was manufactured at 350 °C for 0.25 h, while the neutral (pH 7.02) and alkali (pH 11.21) rice husk biochars were produced at 450 °C for 0.25 h and 600 °C for 0.50 h, respectively. The rice husk biochars classified by their pH values were ground and sieved through a 53 μm mesh, as reported on a micron-scale (< 0.53 μm), to differentiate their forms (i.e., micron-scale and sub-centimeter)[50]. In this study, to clearly distinguish between the pH of the neutral and alkali rice husk biochars, it was necessary to extend the pyrolysis time by a factor of two.

To prepare the experimental solution with the varying concentration of NH_4^+, ammonium chloride (NH_4Cl, Assay 99% (Extra pure), Daejung chemicals & Metals, Gyeonggi, South Korea) was dissolved in secondary distilled water. The varying NH_4^+ concentrations (i.e., 0.01, 0.05, 0.10, 0.20, 0.50, and 1.00 g L^{-1}) of the

experimental solution were attained by diluting the initial experimental solution of 1.00 ± 0.02 g NH_4^+ L^{-1} with secondary distilled water. The pH of the experimental solution was adjusted to a range of pH 6.5–7.0 using 0.1 M hydrochloric acid (HCl, Assay 37% (Guaranteed reagent), Daejung chemicals & Metals, Gyeonggi, South Korea) and sodium hydroxide (NaOH, Assay 97% (Extra pure), Daejung chemicals & Metals, Gyeonggi, South Korea).

Adsorption kinetic experiments

For the Adsorption kinetic experiments of the rice husk biochars, 0.50 g of the rice husk biochars were placed into a 50 mL centrifuge tube containing 40 mL of experimental solution at a concentration of 0.10 g NH_4^+ L^{-1}, and these experiments conducted at room temperature condition (25 ± 1 °C). In this study, the dosage of the rice husk biochar was set as the maximum level that could prevent the overlapping effects of adsorbent, as reported in previous study[51]. The mixture of the rice husk biochar and NH_4^+ solution was then shaking at 210 rpm using an electrical shaker. Subsamples were obtained at specific intervals of 0.5, 1.0, 2.0, 4.0, 8.0 and 16.0 h. After the subsamples were filtered, the residual NH_4^+ concentrations of the subsamples were determined by a UV/Vis-spectrophotometer basis on the Indophenol blue method (640 nm). The concentrations of NH_4^+ adsorbed by the rice husk biochars were calculated using Eq. 3, while the NH_4^+ removal (%) was estimated by Eq. 4.

$$Q_t = (C_o - C_e) \times V / W \tag{3}$$

$$NH_4^+ \text{ removal } (\%) = (C_o - C_e) / C_o \times 100 \tag{4}$$

Where, Q_t denotes the amount of NH_4^+ adsorbed by the rice husk biochar at a specific interval (mg g^{-1}). C_o represents the initial concentration of the NH_4^+ solution (mg L^{-1}), while C_e is the residual NH_4^+ concentration of the experimental solution at a specific interval (mg L^{-1}). V and W denote the volume of the NH_4^+ solution (L) and mass of the rice husk biochars (g), respectively.

In this study, to evaluate the adsorption rate of the rice husk biochar according to the reaction time, two typical kinetic models (i.e., pseudo-first-order model and pseudo-second-order model) were used. The PFO and PSO kinetic models were employed to describe the NH_4^+ adsorption rate of the rice husk biochar with respect to reaction time and represented in Eq. 5 and Eq. 6.

$$\ln (Q_e - Q_t/Q_e) = -K_1 \times t \tag{5}$$

$$t / Q_t = 1 / K_2 \times {Q_e}^2 + t / Q_e \tag{6}$$

Where, Q_e denotes the total amount of NH_4^+ adsorbed by the rice husk biochar (mg g^{-1}). t is the reaction time (h), while K_1 and K_2 denote the kinetic constant of PFO (h^{-1}) and PSO (g mg^{-1} h^{-1}) kinetic models, respectively. Adsorption kinetic experiments in this study were conducted in triplicate.

Adsorption capacity experiments

In this study, adsorption isotherms are used to depict the interaction and mechanism between the rice husk biochar and NH_4^+at equilibrium state[12]. The Langmuir and Freundlich isotherms, which were considered the representative adsorption isotherm, were employed to evaluate the experimental results, including the adsorbed amount of $NH_4^+$by the rice husk biochar, initial adsorption rate, and coefficient of determination (R^2). The linear forms of the Langmuir and Freundlich isotherms used in this adsorption capacity experiment were represented in Eq. 7 and Eq. 8, respectively. The Freundlich isotherm is commonly used to describe the chemical adsorption of biochar on heterogeneous surfaces, while the Langmuir isotherm can be employed to depict the monolayer adsorption of NH_4^+ solutions on the biochar

$$Q_t = -Q_t / b \times C_e + Q_m \tag{7}$$

$$\ln (Q_t) = \ln (K_F) + 1/n \times \ln (C_e) \tag{8}$$

Where, Q_m denotes the monolayer adsorption capacity of NH_4^+ by the rice husk biochar (mg g^{-1}), while b represents the binding capacity of the rice husk biochars (L mg^{-1}). K_F and n exhibit the adsorption capacity constant and adsorption intensity constant in the Freundlich isotherm, respectively.

For the NH_4^+ adsorption capacity experiments of the rice husk biochars, the rice husk biochars were weighted using an electrical balance and placed into a 50 mL centrifuge cube containing 40 mL of experimental solution at a concentration of 0.10 g NH_4^+ L^{-1}. The dosage of the rice husk biochars were set at 0.004, 0.02, 0.04, 0.2, 0.4, 1.2, and 2.0 g, which were 0.10, 0.50, 1.00, 5.00, 10.00, 30.00, and 50.00 g L^{-1} in the experimental solution, respectively. The mixed slurry samples were vibrated at 210 rpm using an electrical shaker and filtered by a Whatman qualitative filter paper no. 1. The collected supernatant was analyzed to quantify the residual NH_4^+ concentration in the experimental solution using a UV/Vis-spectrophotometer basis on the Indophenol blue method (640 nm). Adsorption capacity experiments in this study were conducted at room temperature (25 ± 1 °C) and in triplicate.

Characterization of rice husk biochar

The pH and electrical conductivity (EC) of the rice husk biochars were measured in a biochar slurry, where 5 g of the rice husk biochars was blended with 50 mL of secondary distilled water, using a Benchtop Meter equipped with pH and EC potables (ORION™ Versa Star Pro ™, Thermo Scientific Inc., Waltham, Massachusetts, USA). The Brunner-Emmett-Teller (BET) surface area of the rice husk biochars was measured using the N gas-adsorption method with a Surface area analyzer (ASAP 2420, Micromeritics Inc., Norcross, Georgia, USA).

The Total carbon (C), nitrogen (N), hydrogen (H), and oxygen (O) contents of the rice husk biochars were analyzed by an elemental analyzer (TruSpec Micro, Leco Corp., Michigan, USA). Total phosphorus (P) content was assessed using the vanadate molybdate method with a UV/Vis-spectrophotometer (GENESYS 50, Thermo Scientific Inc., Waltham, Massachusetts, USA). The functional groups of the rice husk biochars were determined by a Fourier transform infrared spectroscopy (FT-IR, Spectrum Two, Perkin Elmer, Waltham, Massachusetts, USA). To evaluate the stability and polarity of the rice husk biochars, the elemental contents were used to calculate the H: C ratio and O: C ratio.

Statistical analysis

All adsorption kinetic and capacity experiments were conducted in triplicate. The statistical relationship between the adsorption characteristics of NH_4^+ by the rice husk biochars and experimental conditions (e.g., chemical properties of the rice husk biochars, reaction time, and initial concentration) was evaluated by a statistical software (IBM SPSS Statistics 26, New York, USA). Additionally, the experimental data were subjected to analysis of variance (ANOVA), and means were compared using Duncan's multiple range test.

Data availability

All data generated or analyzed during this study are included in this published article [and its supplementary materials].

Received: 19 May 2024; Accepted: 22 November 2024
Published online: 02 December 2024

References

1. Chen, L. et al. Comparison of Nitrogen loss weight in Ammonia Volatilization, Runoff, and leaching between common and slow-release fertilizer in Paddy Field. *Wat Air Soil. Poll.* **232**, 132. https://doi.org/10.1007/s11270-021-05083-6 (2021).
2. Cai, Y., Qi, H., Liu, Y. & He, X. Sorption/desorption behaviour and mechanism of NH_4^+ by biochar as a nitrogen fertilizer sustained-release material. *J. Agric. Food Chem.* **64**, 4958–4964. https://doi.org/10.1021/acs.jafc.6b00109 (2016).
3. He, Z. et al. Nitrate adsorption and desorption by Biochar. *Agron* **13**, 2440. https://doi.org/10.3390/agronomy13092440 (2023).
4. Igwegbe, C. A., Kozlowski, M., Wasowicz, J., Peczek, E. & Bialowiec, A. Nitrogen removal from Landfill Leachate using Biochar Derived from Wheat Straw. *Mater* **17**, 928. https://doi.org/10.3390/ma17040928 (2024).
5. Schulte-Uebbing, L. F., Beusen, A. H. W., Bouwman, A. F. & de Vries, W. From planetary to regional boundaries for agricultural nitrogen pollution. *Nat* **610**, 507–512. https://doi.org/10.1038/s41586-022-05158-2 (2022).
6. Kang, Y. G. et al. Pyrolysis temperature and time of rice husk biochar potentially control ammonia emissions and Chinese cabbage yield from urea-fertilized soils. *Sci. Rep.* **14**, 5692. https://doi.org/10.1038/s41598-024-54307-2 (2024).
7. Begum, S. A., Golam Hyder, A. H. M., Hicklen, Q., Crocker, T. & Oni, B. Adsorption characteristics of ammonium onto biochar from an aqueous solution. *AUOA Water Infrastruct. Ecosyst. Soc.* **70**, 113–122. https://doi.org/10.2166/aqua.2020.062 (2021).
8. Huang, J. et al. Removing ammonium from water and wastewater using cost-effective adsorbents: a review. *J. Environ. Sci.* **63**, 174–197. https://doi.org/10.1016/j.jes.2017.09.009 (2018).
9. Han, B., Butterly, C., Zhang, W., He, J. Z. & Chen, D. Adsorbent materials for ammonium and ammonia removal: a review. *J. Clean. Prod.* **283**, 124611. https://doi.org/10.1016/j.jclepro.2020.124611 (2021).
10. Lv, R. et al. Adsorption and leaching characteristics of ammonium and nitrate from paddy soil as affected by biochar amendment. *Plant. Soil. Environ.* **67**, 8–17. https://doi.org/10.17221/276/2020-PSE (2021).
11. Fidel, R. B., Laird, D. A. & Spokas, K. A. Sorption of ammonium and nitrate to biochars is electrostatic and pH-dependent. *Sci. Rep.* **8**, 17627. https://doi.org/10.1038/s41598-018-35534-w (2018).
12. Chen, M., Wang, F., Zhang, D. I., Yi, W. M. & Liu, Y. Effects of acid modification on the structure and adsorption NH_4^+-N properties of biochar. *Renew. Energy*. **169**, 1343–1350. https://doi.org/10.1016/j.renene.2021.01.098 (2021).
13. Halder, P. et al. Ammonium nitrogen (NH_4^+-N) recovery from synthetic wastewater using biosolids-derived biochar. *Bioresour Technol. Rep.* **23**, 101592. https://doi.org/10.1016/j.biteb.2023.101592 (2023).
14. Yang, H. I. et al. Adsorption of ammonium in aqueous solutions by pine sawdust and wheat straw biochars. *Environ. Sci. Poll. Res.* **25**, 25638–25647. https://doi.org/10.1007/s11356-017-8551-2 (2018).
15. Kang, Y. G. et al. Effect of pyrolysis conditions on chemical properties of carbonized rice husks for efficient NH_4^+ adsorption. *Appl. Biol. Chem.* **66**, 45. https://doi.org/10.1186/s13765-023-00806-1 (2023).
16. Kizito, S. et al. Evaluation of slow pyrolyzed wood and rice husks biochar for adsorption of ammonium nitrogen from piggery manure anaerobic digestate slurry. *Sci. Total Environ.* **505**, 102–112. https://doi.org/10.1016/j.scitotenv.2014.09.096 (2015).
17. Hou, J. et al. Adsorption of ammonium on biochar prepared from giant reed. *Environ. Sci. Poll. Res.* **23**, 19107–19115. https://doi.org/10.1007/s11356-016-7084-4 (2016).
18. Kang, Y. G., Lee, J. H., Chun, J. H. & Oh, T. K. Adsorption characteristics of NH_4^+ by Biochar Derived from Rice and Maize Residue. *Korean J. Environ. Agric.* **40**, 161168. https://doi.org/10.5338/KJEA.2021.40.3.19 (2021).
19. Kang, Y. G. et al. Adsorption characteristics of NH_4-N by biochar derived from pine needles. *Korean J. Agric. Sci.* **48**, 589–596. https://doi.org/10.7744/kjoas.2021004 (2021).
20. Wang, Z. et al. Biochar produced from oak sawdust by Lanthanum (La)-involved pyrolysis for adsorption of ammonium (NH_4^+), nitrate (NO_3^-), and phosphate (PO_4^{3-}). *Chemosphere* **119**, 646–653. https://doi.org/10.1016/j.chemosphere.2014.07.084 (2015).
21. Wang, Z. et al. Characterization of Acid-Aged Biochar and its ammonium adsorption in an aqueous solution. *Mater* **13**, 2270. https://doi.org/10.3390/ma13102270 (2020).
22. Gai, X. et al. Effects of feedstock and pyrolysis temperature on biochar adsorption of ammonium and nitrate. *PLOS ONE.* **9**, 2113888. https://doi.org/10.1371/journal.pone.0113888 (2014).
23. Yin, Q., Zhang, B., Wang, R. & Zhao, Z. Phosphate and ammonium adsorption of sesame straw biochars produced at different pyrolysis temperature. *Environ. Sci. Poll. Res.* **25**, 4320–4329. https://doi.org/10.1007/s11356-017-0778-4 (2018).
24. Zhang, Y., Li, Z. & Mahmood, I. B. Recovery of NH4 + by corn cob produced biochars and its potential application as soil conditioner. *Front. Environ. Sci. Eng.* **8**, 825–834. https://doi.org/10.1007/s11783-014-0682-9 (2014).
25. Choi, J. W., Choi, D. H., Cho, T. S. & Meier, D. Characterization of bio-oils produced by Fluidized Bed type fast pyrolysis of Woody Biomass. *J. Korean Wood Sci. Technol.* **34**, 36–43. https://doi.org/10.5658/WOOD.2006.34.6.36 (2006).
26. Abrishamkesh, S., Gorji, M., Asadi, H., Bagheri-Marandi, G. H. & Pourbabaee, A. A. Effects of rice husk biochar application on the properties of alkaline soil and lentil growth. *Plant. Soil. Environ.* **61**, 475–482. https://doi.org/10.17221/117/2015-PSE (2015).
27. Chandra, S. & Bhattacharya, J. Influence of temperature and duration of pyrolysis on the property heterogeneity of rice straw biochar and optimization of pyrolysis conditions for its application in soils. *J. Clean. Prod.* **215**, 1123–1139. https://doi.org/10.1016/j.jclepro.2019.01.079 (2019).

28. Paethanom, A. & Yoshikawa, K. Influence of Pyrolysis temperature on Rice Husk Char characteristics and its Tar Adsorption Capacity. *Energies* **5**, 4941–4951. https://doi.org/10.3390/en5124941 (2012).
29. Huang, Y., Jin, B., Zhong, Z., Zhong, W. & Xiao, R. Characteristics and mercury adsorption of activated carbon produced by CO_2 of chicken waste. *J. Environ. Sci.* **20**, 291–296. https://doi.org/10.1016/S1001-0742(08)60046-7 (2008).
30. Chen, J., Fang, D. & Duan, F. Pore characteristics and fractal properties of biochar obtained from the pyrolysis of coarse wood in a fluidized-bed reactor. *Appl. Ener*. **218**, 54–65. https://doi.org/10.1016/j.apenergy.2018.02.179 (2018).
31. Jassal, R. S. et al. Nitrogen enrichment potential of biochar in relation to pyrolysis temperature and feedstock quality. *J. Environ. Manag*. **152**, 140–144. https://doi.org/10.1016/j.jenvman.2015.01.021 (2015).
32. Keiluweit, M., Nico, P. S., Johnson, M. G. & Kleber, M. Dynamic molecular structure of plant biomass-derived black carbon (Biochar). *Environ. Sci. Technol.* **44**, 1247–1253. https://doi.org/10.1021/es9031419 (2010).
33. Al-Wabel, M. I., Al-Omran, A., El-Naggar, A. H., Nadeem, M. & Usman, A. R. A. Pyrolysis temperature induced changes in characteristics and chemical composition of biochar produced from conocarpus wastes. *Bioresour Technol.* **131**, 374–379. https://doi.org/10.1016/j.biortech.2012.12.165 (2013).
34. Karam, D. S. et al. An overview on the preparation of rice husk biochar, factors affecting its properties, and its agriculture application. *J. Saudi Soc. Agric. Sci.* **21**, 149–159. https://doi.org/10.1016/j.jssas.2021.07.005 (2022).
35. Ippolito, J. A. et al. Feedstock choice, pyrolysis temperature and type influence biochar characteristics: a comprehensive meta-data analysis review. *Biochar* **2**, 4. https://doi.org/10.1007/s42773-020-00067-x (2020).
36. Claoston, N., Samsuri, A. W., Ahmad Husni, M. H. & Mohd Amran, M. S. Effects of pyrolysis temperature on the physicochemical properties of empty fruit bunch and rice husk biochars. *Waste Manage. Res.* **32**, 331–339. https://doi.org/10.1177/0734242X145258 (2014).
37. Guo, X. et al. Adsorption mechanism of Hexavalent Chromium on Biochar: kinetic, thermodynamic, and characterization studies. *ACS Omega*. **42**, 27323–27331. https://doi.org/10.1021/acsomega.0c03652 (2020).
38. He, Z. et al. Effects of biochar particle size on sorption and desorption behavior of NH_4^+-N. *Ind. Crops Prod.* **189**, 115837. https://doi.org/10.1016/j.indcrop.2022.115837 (2022).
39. Jin, Z. et al. Adsorption and catalytic degradation of organic contaminants by biochar: overlooked role of biochar's particle size. *J. Hazard. Mater.* **422**, 126928. https://doi.org/10.1016/j.jhazmat.2021.126928 (2022).
40. Wei, L. et al. Biochar characteristics produced from rice husks and their sorption properties for the acetanilide herbicide metolachlor. *Environ. Sci. Poll. Res.* **24**, 4552–4561. https://doi.org/10.1007/s11356-016-8192-x (2017).
41. Sharmila, V. G., Tyagi, V. K., Varjani, S. & Banu, J. R. A review on the lignocellulosic derived biochar-based catalyst in wastewater remediation: Advanced treatment technologies and machine learning tools. *Bioresour Technol.* **387**, 129587. https://doi.org/10.1016/j.biortech.2023.129587 (2023).
42. Bhandari, G. et al. Nano-biochar: recent progress, challenges, and opportunities for sustainable environmental remediation. *Front. Micobiol*. **14**, 1214870. https://doi.org/10.3389/fmicb.2023.1214870 (2023).
43. Zhang, K., Mao, J. & Chen, B. Reconsideration of heterostructures of biochars: morphology, particle size, elemental composition, reactivity and toxicity. *Environ. Pollut*. **254**, 113017. https://doi.org/10.1016/j.envpol.2019.113017 (2019).
44. Rajput, V. D. et al. Nano-biochar: a novel solution for sustainable agriculture and environmental remediation. *Environ. Res.* **210**, 112891. https://doi.org/10.1016/j.envres.2022.112891 (2022).
45. Xiang, L. et al. Potential hazards of biochar: the negative environmental impacts of biochar applications. *J. Hazard. Mater.* **420**, 126611. https://doi.org/10.1016/j.jhazmat.2021.126611 (2021).
46. Godlewska, P., Ok, Y. S. & Oleszczuk, P. The Dark side of Black Gold: ecotoxicological aspect of biochar and biochar-amended soils. *J. Hazard. Mater.* **403**, 123833. https://doi.org/10.1016/j.jhazmat.2020.123833 (2021).
47. Lu, T. et al. Pollutant toxicology with respect to microalgae and cyanobacteria. *J. Environ. Sci.* **99**, 175–186. https://doi.org/10.1016/j.jes.2020.06.033 (2021).
48. Zhang, C. et al. Biochar for environmental management: mitigating greenhouse gas emissions, contaminant treatment, and potential negative impacts. *Chem. Eng. J.* **373**, 902–922. https://doi.org/10.1016/j.cej.2019.05.139 (2019).
49. Ang, L. M. & Seng, K. P. Big Sensor Data Applications in Urban environments. *Big Data Res.* **4**, 1–12. https://doi.org/10.1016/j.bdr.2015.12.003 (2016).
50. Ma, S., Jing, F., Sohi, S. P. & Chen, J. New insights into contrasting mechanisms for PAE adsorption on millimeter, micron- and nano- scale biochar. *Environ. Sci. Poll. Res.* **26**, 18636–18650. https://doi.org/10.1007/s11356-019-05181-3 (2019).
51. Choi, Y. S., Hong, S. G., Kim, S. C. & Shin, J. D. Adsorption characteristics of aqueous phosphate using Biochar Derived from Oak Tree. *J. Korean Org. Resour. Recycl Assoc.* **23**, 60–67. https://doi.org/10.17137/korrae.2015.23.3.060 (2015).

Author contributions

Yun-Gu Kang, Conceptualization; Methodology; Formal analysis and investigation; Data collection and statistical analysis; Writing - original draft; ResourcesDo-Gyun Park, Conceptualization; Formal analysis and investigation; Data collection and statistical analysis; Writing - original draft; Funding acquisition; ResourcesJun-Yeong Lee, Formal analysis and investigation; Data collection and statistical analysis; Ji-Won Choi, Formal analysis and investigation; Data collection and statistical analysis; Jun-Ho Kim, Formal analysis and investigation; Data collection and statistical analysis; Ji-Hoon Kim, Formal analysis and investigation; Data collection and statistical analysis; Yeo-Uk Yun, Conceptualization; Methodology; Data collection and statistical analysis; Writing - review and editing; Resources; SupervisionTaek-Keun Oh, Conceptualization; Methodology; Writing - original draft; Writing - review and editing; Funding acquisition; Resources; Supervision.

Declarations

Competing interests

The authors declare no competing interests.

Additional information

Supplementary Information The online version contains supplementary material available at https://doi.org/10.1038/s41598-024-80873-6.

Correspondence and requests for materials should be addressed to Y.-U.Y. or T.-K.O.